Jussila, Henri; Albrow-Owen, Tom; Yang, He; Hu, Guohua; Aksimsek, Sinan; Granqvist, Niko; Lipsanen, Harri; Howe, Richard C.T.; Sun, Zhipei; Hasan, Tawfique

New Approach for Thickness Determination of Solution-Deposited Graphene Thin Films

ACS OMEGA

New Approach for Thickness Determination of Solution-Deposited Graphene Thin Films

Henri Jussila,*[†,‡] Tom Albrow-Owen,[†] He Yang,[‡] Guohua Hu,[†] Sinan Aksimsek,[§,‡] Niko Granqvist,[∥] Harri Lipsanen,[‡] Richard C. T. Howe,[†] Zhipei Sun,[‡] and Tawfique Hasan*[†]

[†]Cambridge Graphene Centre, University of Cambridge, 9 JJ Thomson Avenue, Cambridge CB3 0FA, U.K.
[‡]Department of Electronics and Nanoengineering, Aalto University, Tietotie 3, 02150 Espoo, Finland
[§]Department of Electrical and Electronics Engineering, Istanbul Kultur University, Bakırkoy, Istanbul 34156, Turkey
[∥]BioNavis Ltd., Elopellontie 3C, 33470 Ylöjärvi, Finland

S *Supporting Information*

ABSTRACT: Solution processing-based fabrication techniques such as liquid phase exfoliation may enable economically feasible utilization of graphene and related nanomaterials in real-world devices in the near future. However, measurement of the thickness of the thin film structures fabricated by these approaches remains a significant challenge. By using surface plasmon resonance (SPR), a simple, accurate, and quick measurement of the deposited thickness for inkjet-printed graphene thin films is reported here. We show that the SPR technique is convenient and well-suited for the measurement of thin films formulated from nanomaterial inks, even at sub-10 nm thickness. We also demonstrate that the analysis required to obtain results from the SPR measurements is significantly reduced compared to that required for atomic force microscopy (AFM) or stylus profilometer, and much less open to interpretation. The gathered data implies that the film thickness increases linearly with increasing number of printing repetitions. In addition, SPR also reveals the complex refractive index of the printed thin films composed of exfoliated graphene flakes, providing a more rigorous explanation of the optical absorption than that provided by a combination of AFM/profilometer and the extinction coefficient of mechanically exfoliated graphene flakes. Our results suggest that the SPR method may provide a new pathway for the thickness measurement of thin films fabricated from any nanomaterial containing inks.
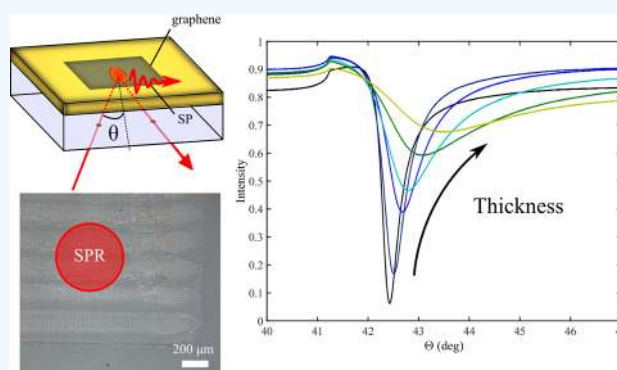
INTRODUCTION

Over the past decade, graphene and other two-dimensional (2d) materials have been extensively studied, attracting considerable interest for a range of applications.[1] This interest, initially directed toward graphene, originates from the various exciting and unique properties that these 2d materials possess (for example, high-mobility,[2,3] ultrafast optical response,[4,5] high thermal conductivity,[6] band gap tunability,[7] or intrinsic anisotropy[8,9]). Many proof-of-concept devices have recently been reported that begin to demonstrate the potential for exploiting these properties.[1] As a result, the current expectation is that many commercial device components developed from such nanomaterials will emerge in the near future. Much research is still needed, however, for this vision to be realized. For instance, it is crucial that not only basic research is conducted but also corresponding progress is simultaneously made in the development of suitable, economically competitive fabrication techniques. The key requirements for such processes are that it is low-cost, scalable, and also compatible with as many different substrate materials as possible. One set

of promising production methods that fulfill these requirements are solution processing-based approaches which formulate nanomaterial-based inks suitable for deposition on a range of substrates with pre-existing graphics/functional printing and coating techniques.[10]

In developing applications that utilize these inks, it is essential to measure the physical properties of the fabricated thin films, including their thickness and uniformity. The current state-of-the-art for semitransparent, solution-deposited thin film thickness determination is either atomic force microscopy[11,12] (AFM) or stylus profilometer. This, however, is a difficult task because of the many complications that arise: (i) thin films deposited in these ways are a collection of small crystal flakes rather than a continuous film, leading to high surface roughness and ambiguity in the true film thickness; (ii) as-deposited thin films rarely form a sharp "step" at their boundary, instead
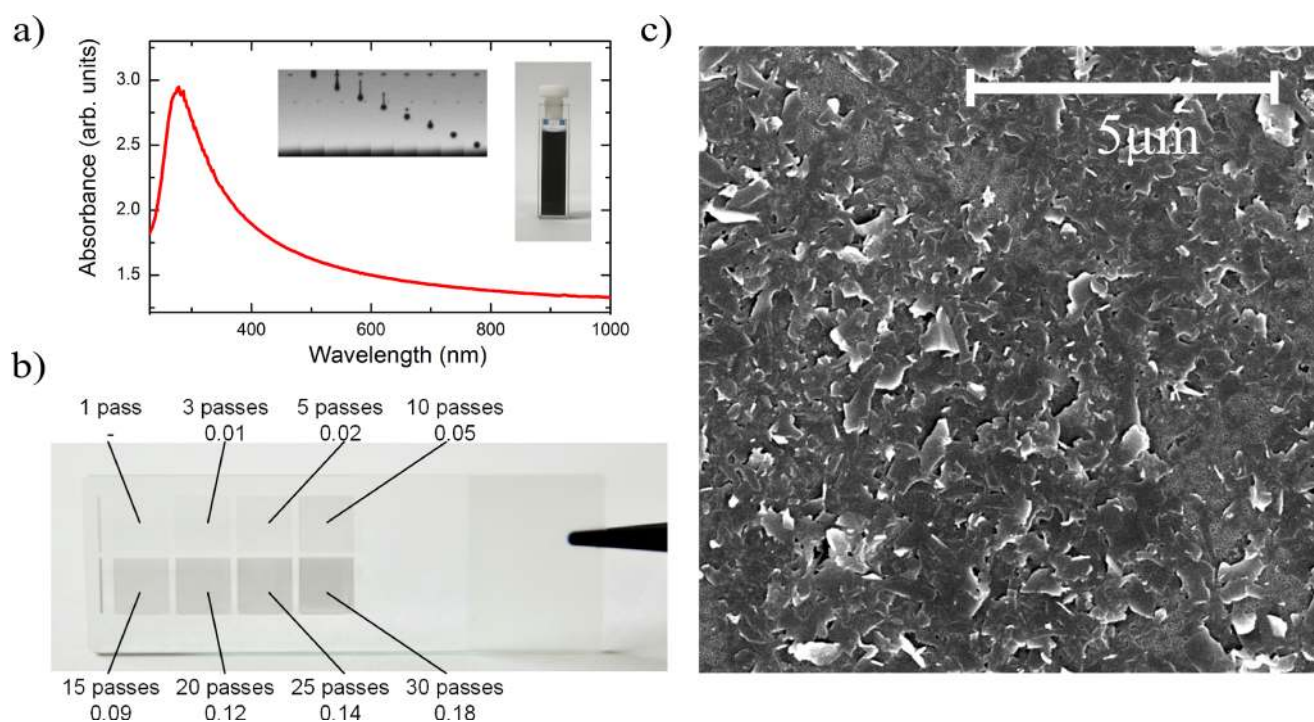
Figure 1. (a) Optical absorption spectrum of the graphene ink. To minimize scattering loss the ink is diluted to 10% v/v for absorbance measurements. Image insets show a cuvette containing the diluted ink and also the droplet jetting sequence of the graphene ink at 0−80 μs after jetting, in 10 μs intervals. (b) Photograph of inkjet-printed graphene films demonstrating a gradual increase in absorbance (absorbance values listed in image) with increasing number of printing passes/repetitions, from 1 to 30 repetitions. (c) Top-view SEM image illustrating the porous nature of the inkjet-printed graphene film (30 printing repetitions) after the removal of the PVP by annealing.

showing a sloped or rounded height profile. This means that at micrometer length scales, there is often no easily-definable 'edge' of the film. Depending on the wetting/drying process of the ink, this edge region with poorly defined thickness may extend for several tens of μm into the film; (iii) physical contact with the thin film by stylus profilometer or contact-mode AFM tip will usually displace or drag material, not only damaging the film, but more importantly, affecting the accuracy of the measurement. This is especially true for thin films without any polymer binder; (iv) the measured thickness is always only a local thickness estimation, and thereby not necessarily a reliable representation of the film as a whole. This is particularly relevant for AFM measurements, where it is only possible to gather data from an area in the order of $100 \times 100 \ \mu m^2$. Thus, there exists a great demand for a rapid, large area, contactless, low-cost, and simple characterization technique for the thickness measurement of solution-deposited nanomaterial thin films.

Surface plasmon resonance (SPR) is a contactless, all-optical analysis technique which is typically used in (bio)sensing applications,[13,14] but can also be used as a method for thin film characterization.[15,16] In SPR measurement, a glass substrate with a noble metal coating (typically silver or gold) is used to couple plasmonic waves inside the measurement substrate.[15] The resonant angle (at which the surface plasmon (SP) excitation occurs), and more generally, the shape of the SPR curve, depend strongly on the conditions at the surface of the measurement substrate, thus allowing the desired information from the sample to be quickly obtained from the SPR curve. Several works with graphene using SPR[17−20] and other applications utilizing plasmonics[21−24] have recently been demonstrated.[1,25] For instance, we have recently shown that

accurate estimation of both the thickness and refractive index of CVD-grown graphene films from the SPR curve is possible, proving that this technique is capable of gathering information from a large sample area ($\sim mm^2$), even for single-atom thick solid layers.[20]

In this work, we report an accurate and simple method to measure the thickness of graphene thin films fabricated by inkjet printing. The structure and surface morphology of these solution-deposited graphene thin films differ considerably from that of a CVD-grown layer and the results demonstrate a new pathway for the thickness measurement of thin films fabricated from nanomaterial containing inks. We also show that the SPR technique is convenient and well suited for the measurement of thin films formulated from nanomaterial inks even at sub-10 nm thicknesses, with improved accuracy compared to that of the more conventional AFM and stylus profilometer based measurement techniques.

■ RESULTS AND DISCUSSION

Ink Characteristics and Printing. Samples for SPR measurements are fabricated by inkjet printing graphene ink on Au-coated SPR sensors with varied numbers of printing repetitions. The graphene ink is prepared via an ultrasonic-assisted liquid phase exfoliation (UALPE) process as described elsewhere.[26] In the UALPE process, bulk graphite crystals are generally first added to a solvent for exfoliation via ultra-sonication. The resultant dispersion is then centrifuged to sediment the unexfoliated graphite, yielding an ink enriched with mono-, few-, and multi-layer graphene. The choice of the solvent defines the exfoliation efficiency and ink stability, with the difference in Hansen solubility parameters (HSPs—a measure of the solvent−graphene intermolecular interac-
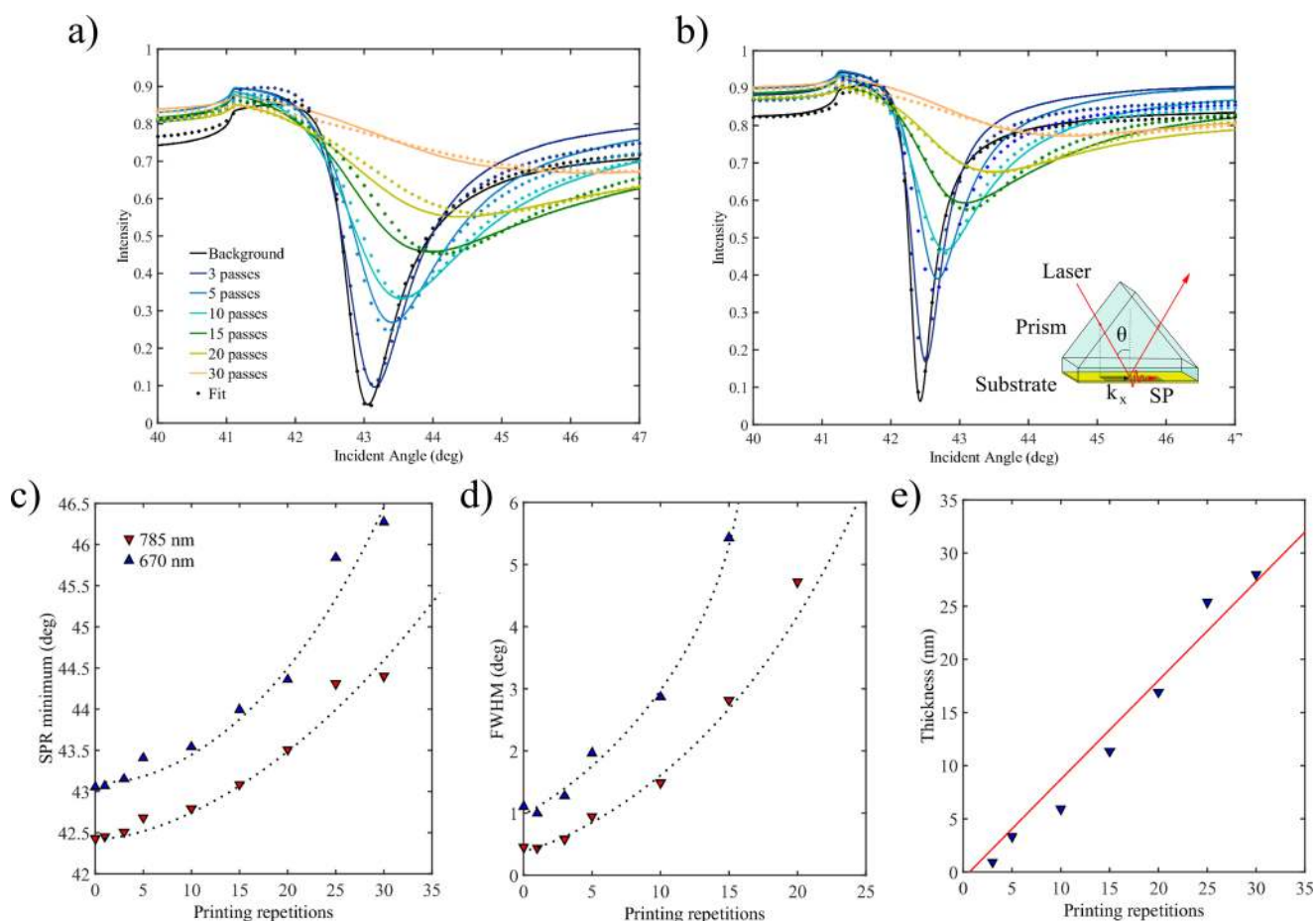
Figure 2. (a, b) SPR curves of inkjet-printed graphene samples measured with the wavelength of 670 and 785 nm, respectively. Fits (marked with ●) were obtained with the method described in the Experimental Methods section. Inset of (b) shows a schematic illustrating the SPR measurement principle. During the measurement, the incident angle of the laser beam is altered causing the wave vector component parallel to the SPR substrate, k_x, to change. When the wave vector matches the wave vector of the SP (which is strongly affected by the materials near the surface of the SPR substrate) SP excitation occurs. (c) SPR resonance angle, (d) full width at half-maximum, and (e) graphene film thickness as a function of printing repetitions. The graphene film thickness was obtained from the fitted SPR curves.

tions)[27,28] between the solvent and graphene providing an empirical measure of solvent suitability. Here, the graphene ink is prepared via UALPE of graphite in isopropyl alcohol (IPA). Due to its low boiling point (82.6 °C) and low surface tension (~23 mN m^{-1}), IPA is well suited to printing techniques such as inkjet printing and spray-coating, allowing good wetting of the substrate and rapid drying of the printed films.[29] However, the mismatch in HSPs between graphene and pure IPA is too great to support a stable dispersion. Therefore, poly-(vinylpyrrolidone) (PVP), a polymer which has previously been used to stabilize dispersions of graphene in IPA,[29] is used as an ink stabilizer. The PVP−IPA-based inks remain stable for several months after preparation without the formation of any visible aggregations.

The graphene ink concentration is estimated to be 0.59 g L^{-1} through optical absorbance spectroscopy, as described in the Experimental Methods section (see Figure 1a). The dispersion is diluted to 10% v/v for this measurement to reduce the effect of scattering.[30] As expected, the absorbance spectrum is mostly featureless due to the linear dispersion of Dirac electrons, with a single peak at ~300 nm, a signature of the van Hove singularity in the graphene density of states.[31] Further characterizations of the graphene flakes, including statistical measurement of the flake thickness and lateral dimensions via

AFM and Raman spectra, are presented in Figure S1. In particular, the AFM measurements demonstrate that the graphene in the dispersion consists of few-layer flakes with an average measured thickness of 7.3 ± 0.3 nm, and 51% of flakes are ≤4 nm or 10 layers thick, assuming a ~0.7 nm measured thickness for a monolayer flake and ~0.35 nm increase for each subsequent layer.[32] The average lateral dimension is 188 ± 6 nm.

Next, the fluidic properties of the graphene ink for inkjet printing are assessed. Inkjet inks are typically described in terms of the dimensionless figure of merit $Z = \sqrt{\gamma \rho a}/\mu$, where γ, ρ, and μ are the ink surface tension (mN m^{-1}), density (g cm^{-3}), and viscosity (mPa·s), respectively, and a is the inkjet nozzle diameter (μm).[33] The preferred range for stable jetting is $1 < Z < 14$, with $Z < 1$ failing to jet, and $Z > 14$ producing undesired satellite droplets. Achieving stable jetting with a single droplet for each jetting impulse is of primary importance for inkjet printing, ensuring that the ink is uniformly deposited on to the substrate, but only in desired areas. The ink in this work has $\gamma \sim 28$ mN m^{-1}, $\mu \sim 2.4$ mPa·s, and $\rho \sim 0.8$ g cm^{-3}, and the printer (Fujifilm Dimatix DMP-2381) uses cartridges with $a = 22$ μm. This gives a Z value of ~9.2, indicating that the graphene ink is suitable for inkjet printing. This allows the printing process to occur without the formation of unwanted

satellite droplets.[26,29] This was confirmed by the printer stroboscopic camera, which showed a stable droplet jetting sequence (see the inset of Figure 1a). Figure 1b shows inkjet-printed graphene squares on microscope glass slides with printing repetitions varied from 1 to 30. The absorbance of the printed graphene films (listed in the inset for each graphene square) increases linearly with increasing number of printing repetitions. Also, as can be seen from the image, the printed patterns are highly uniform with well-defined edges, further demonstrating that the ink jetting and wetting properties are well tuned for this printing process.

After inkjet printing, the samples shown in Figure 1b are heated at 400 °C for 30 min to decompose and remove the PVP polymer stabilizer.[34] Note that the PVP decomposition step is also performed on those samples used in the SPR measurements, discussed later in this work. To verify that the 400 °C annealing step does not affect the quality of the printed graphene layer, Raman measurements are also performed after the annealing step (also shown in Figure S1). As described, both the spectra (pre- and post-annealing) indicate that the graphene is not affected by the annealing process. However, the removal of PVP leaves the printed film as a porous graphene structure, with large fractions of the volume previously filled by the polymer now consisting of air. This porosity and the air content is further evidenced by SEM imaging of the printed graphene (shown in Figure 1c), which clearly shows air gaps within the thin film. Based on the concentrations of PVP and graphene in our ink, we estimate that PVP could even comprise ~50% of the total volume of the printed film before the annealing step, assuming the density of graphene is equal to that of graphite (2.3 g cm^{-3}). However, the density of the bulk graphite crystals may differ from the density of exfoliated graphene flakes (~0.03–0.4 g cm^{-3}),[26] which would give a lower volume fraction for PVP. Simultaneously, the thickness of our thin film reduces when the annealing step is performed, also affecting the actual composition of the film after the annealing step. Note that, neglecting the possibility of any air present in the film, the flake-to-flake distance after the PVP decomposition step would not be the same as that in perfectly aligned graphite crystals or mechanically exfoliated graphene flakes. All these factors introduce a considerable uncertainty in our estimations of the thin film composition. Even so, it can still be concluded that the remaining graphene structure is porous in nature, physically different from the perfectly crystalline graphene/graphite crystals; and contains a significant fraction of air by volume.

SPR Measurements. The SPR measurements of the inkjet-printed graphene samples are performed in the Kretschmann configuration. Figure 2a,b show typical SPR curves measured from a series of inkjet-printed graphene samples at 670 and 785 nm wavelengths, respectively. In addition, the SPR spectra of a plain reference sample are also shown. To explain the SPR results, the inset of Figure 2b illustrates the SPR measurement principle. In SPR measurement, the incident angle (θ) at which the laser hits the substrate is altered, changing the wave vector component of the incident light parallel to the substrate, k_x. The SP excitation occurs when the wave vector component matches the wave vector of the SP.[15] The wave vector of the SP is strongly affected by the conditions near the gold/dielectric boundary; therefore, the SPR curve of inkjet-printed graphene shows pronounced changes corresponding to the variation in the film thickness. The general trend seen in Figure 2c,d is that the SPR angle increases, along with the broadening of the

resonance as the printing repetition increases (i.e., increased thickness of graphene thin film). This is a typical behavior in SPR measurements when they are performed on a material which absorbs light. Indeed, the SPR angles measured for the 670 nm laser excitation are 43.42, 43.55, 44.41, and 46.58° for 5, 10, 20, and 30 printing repetitions, respectively. Given that the SPR angle of the reference sample is 43.05°, the above shift in the SPR angle is nonlinear. For the 785 nm laser excitation, the SPR resonance angles are 42.43, 42.68, 42.80, 43.53, and 44.54° with 0, 5, 10, 20, and 30 printing repetitions, respectively. At this wavelength, the SPR angle shift is also nonlinear and slightly smaller (~2.1°) than that measured for the 670 nm excitation (~3.5°) for films with 30 printing repetitions.

Because both the complex refractive index and the thickness of the graphene film affect the SPR angle, the optical information from the SPR curves is obtained by fitting the calculated SPR curves to the measurements using the method described in the Experimental Methods section. Note that we perform the fitting process by assuming the same refractive index of graphene for both the 670 and 785 nm wavelengths. This assumption, which reduces the number of fitting parameters, is justified as the refractive index of graphene is almost constant in the visible/near infrared range.[20,31,35−37] As shown in Figure 2, the fitted curves agree well with the measurements. The information obtained by fitting (listed in Table 1 and also shown in Figure 2e) reveals that the thickness of the graphene film increases linearly by ~0.95 nm per printing repetition. This linear increase is desired because it allows the layer thickness to be controlled by the number of printing repetitions and agrees well with previous observations for an optimally working printing process.[11] To reduce the effect of the small changes in the refractive index (between the samples with different numbers of printing repetitions) to the fitted layer thickness, a fitting analysis is also performed by assuming a similar refractive index for all the different samples (fitted curves shown in Figure S2). In this way, the difference between the fitted curves only originates from the changes in the graphene film thickness; and similarly, this fitting technique reveals a refractive index value, which represents an average refractive index of all the printed graphene samples. As a result, the reliability of the fitting technique could be further estimated by comparing the parameters obtained by separate fitting with the set of parameters calculated by the combined fitting method presented in Table S1. As observed, the globally fitted thicknesses and the refractive index agree reasonably well with the separately fitted values, providing further evidence of the reliability of the values listed in Table 1.

The complex refractive index of the printed graphene thin film can also be obtained from the fits. The fitted optical constants are presented in Table 1. It can be seen that the refractive index of the graphene film slowly increases with the increasing number of printing repetitions but is still very close to the refractive index of air (the largest refractive index is 1.158). Also, the global fitting method reveals a refractive index of ~1.12, which is close to all separately fitted refractive index values. We note that the experimentally measured refractive indices of micromechanically exfoliated graphene flakes and CVD graphene films typically range between 2.6 and 3.[20,31,35−37] The refractive index of inkjet-printed graphene measured by SPR is, therefore, significantly smaller. A similar observation can be made for the extinction coefficient, which is observed to be ~0.50. The literature value for the extinction

Table 1. Information Obtained from the SPR Curves by Fitting[a]

| printing repetitions | SPR measurement | | | profilometer | AFM |
	thickness (nm)	n	k	thickness (nm)	thickness (nm)
3	0.94	1.026	0.457	11.6	1.37
5	3.33	1.066	0.549	12.4	2.99
10	5.93	1.101	0.476	21.1	19.5
15	11.36	1.150	0.451	[b]	21.9
20	16.93	1.103	0.474	30.6	22.4
25	25.37	1.158	0.455	38.9	29.6
30	28.01	1.097	0.547	39.2	43.9

[a]Stylus profilometer and AFM measured film thicknesses are also listed. [b]Baseline of the sample too noisy for successful stylus profilometer measurement.

coefficient of micromechanically exfoliated graphene flakes and CVD graphene layers is typically ~1.4.[31,35−37]

The difference in the optical constants between the literature values and the SPR results can be explained by the dissimilarities between the inkjet-printed graphene thin film and single- or few-graphene layers of CVD or exfoliated samples. Though the inkjet-printed graphene film is mainly composed of few-layer thick graphene flakes (see the Figure S1) which, when taken in isolation, are expected to have a refractive index similar to that reported in the literature, the printed film as a whole is porous due to the reasons explained above. It is therefore not surprising that the average refractive index of our inkjet-printed graphene thin film is notably smaller. Indeed, a similar observation has been made for porous silicon and mesoporous silica with refractive indices of ~1.4 and ~1.07, respectively, significantly smaller than the refractive index of their bulk counterparts (3.44 and 1.47 at 670 nm).[38,39] Thus, the refractive index or the extinction coefficient of an inkjet-printed graphene film could be used as a measure of its printing uniformity/porosity. For instance, by comparing the measured extinction coefficient to the literature values, our inkjet-printed graphene thin film absorbs between 30 and 50% of the amount that a similar thickness of single layer graphene would absorb. This also indicates that the graphene film after the PVP decomposition step is porous in nature either due to a large >50% air content and/or due to exfoliated graphene flakes locating further apart from each other (compared to perfectly aligned graphite crystals), thus agreeing with the previous porosity discussion.

AFM and Stylus Profilometer for Inkjet-Printed Graphene Thickness Determination. To compare the thickness values estimated using SPR with those obtained by conventional methods, AFM and stylus profilometer measurements are performed on the sample shown in Figure 1b. The results of these experiments are presented in Figure 3 and listed in Table 1. Figure 3a shows three different profilometer line profiles measured from a sample with 10 printing repetitions from the locations illustrated in the inset. Averaging the height of each line scan with respect to the baseline of the substrate
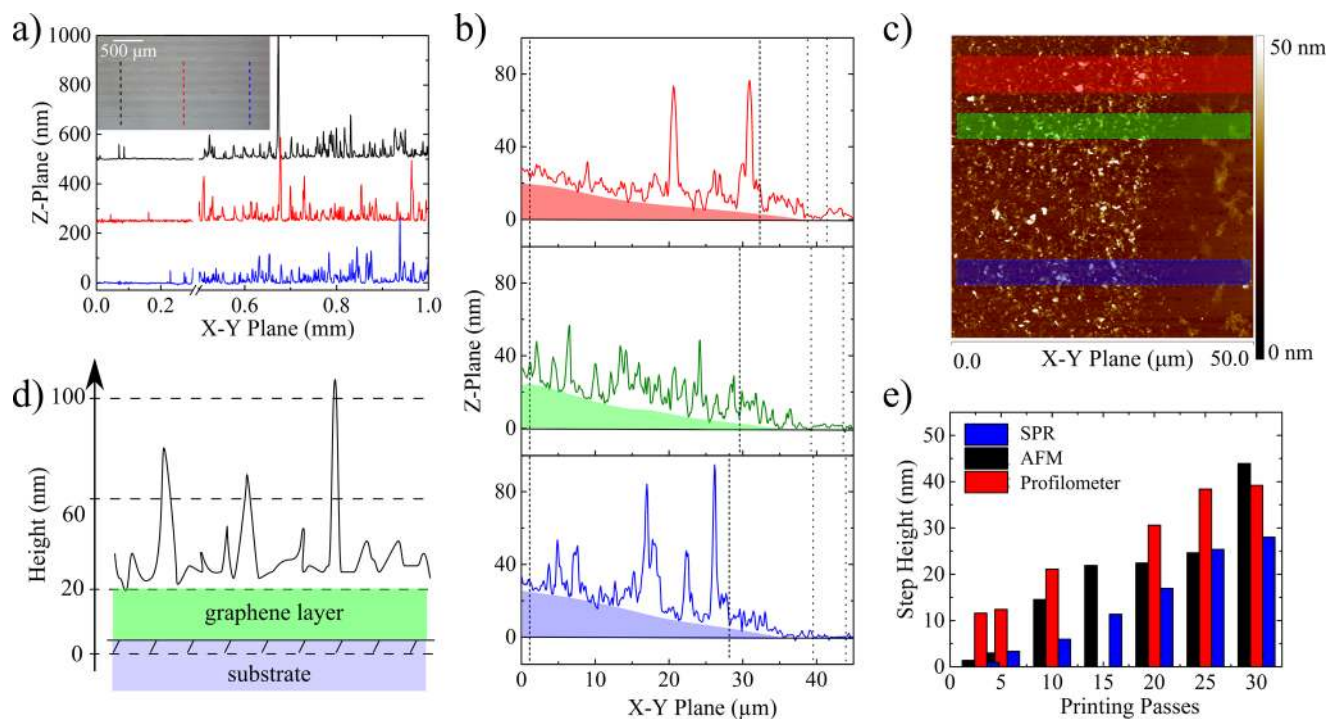

Figure 3. Inkjet-printed graphene film thickness measurements using AFM and stylus profilometer. (a, b) Three different stylus profilometer and AFM measured line scans of the graphene sample fabricated by printing 10 and 20 repetitions of graphene ink, respectively. Inset of (a) shows an optical microscope image of different measurement spots. The graphene film (in (b)) is schematically highlighted with different colors to illustrate its presence. (c) AFM image from the same graphene sample as that shown in (b). (d) Differences between the averaging processes of different measurement techniques. The layer model used in the analysis of SPR measurement assumes an average refractive index at every different distance from the substrate/graphene interface, thus giving smaller weight to surface roughness. For stylus profilometer and AFM measurements, the averaging is performed summing the measured height at each measurement position, thereby giving as much weight to thick aggregated flakes as to the values recorded from the flatter places. (e) Comparison between the AFM, stylus profilometer, and SPR measured graphene film thicknesses as a function of printing repetitions.

gives film thicknesses of 24.1, 21.6, and 17.7 nm for each measurement, demonstrating that the thickness measurement of the thin film differs significantly (>30%) depending on the location of the section measured. A similar observation can also be made from the AFM measurements (see Figure 3b). Once again, the measured thickness is highly dependent on the location. AFM measurements of the sample with 20 printing repetitions are 18.7, 21.3, and 27.1 nm along the red, green, and blue lines shown in Figure 3c. In contrast to SPR measurements, this type of variation is typical for profilometry and AFM measurements of such nanostructured printed thin films and exemplifies how these results may depend on the interpretation and judgment of the user. This highlights the difficulties present for such measurements by AFM and stylus profilometer.

To make these AFM and stylus profilometer measurements better take account of the local thickness variations, we plotted an average of the measurement values gathered from a few different locations in Figure 3e. We note that by increasing the sample size, the effect of local thickness variations can be reduced. However, this simultaneously increases the time required for the measurement. Using this averaging scheme, a thickness value of 21.1 nm can be obtained for an inkjet-printed graphene thin film with 10 printing repetitions with the stylus profilometer. On the other hand, the thickness of the same sample is only ∼6 nm when it is measured by SPR and 19.5 nm when measured by AFM. For the sample with 20 printing repetitions, the thin film thickness is 17 and 22 nm when measured with SPR and AFM, respectively, but 30 nm when measured with the stylus profilometer. This shows that considerable variations exist in thickness estimations between the measurement methods. Therefore, the selection of the measurement spot and sample size used in the averaging process still has an effect, even after the averaging has been performed from millimeter long line scans and multiple different locations. To get a better idea of the comparative size of the measurement areas, see Figure S3.

To highlight the differences between the measurement methods, we fit a first-order curve to the results listed in Table 1. This gives a ∼1.46 and ∼1.26 nm thickness increase per printing repetition for the stylus profilometer and AFM, respectively. Comparing this to the thickness increase of 0.95 nm per printing repetition observed using SPR, we suggest that the stylus profilometer and AFM overestimate (by a factor of ∼1.5 and ∼1.3, respectively) the average thickness for our inkjet-printed graphene thin films. The fact that SPR reveals a smaller thickness than the stylus profilometer and AFM is due to the presence of isolated overlaid flakes, which are visible in the AFM images as large spikes in the line profiles (see Figure 3). The contribution of these features to the SPR measurement is small, given that when considering the horizontal cross-section of the film, the further we rise above the substrate/film interface, the greater the proportion of air with respect to graphene (compare the horizontal lines at the distances of 20, 60, and 100 nm from the graphene/substrate interface in the schematically drawn sample cross-section shown in Figure 3d). Therefore, these thicker regions of the printed film can be effectively considered to represent only "optically denser" air in the SPR layer model. As a result, these thick regions do not as such contribute to the SPR measured thickness of the graphene layer (which in this exemplary case would be ∼20 nm). For AFM and profilometry, however, these spikes would strongly contribute to the overall measurement which is taken as the mean of the measured heights within the printed film (increasing the measured average value of the film thickness in Figure 3d to a significantly larger value than 20 nm).

Inkjet-Printed Graphene Thin Film Absorbance. Finally, to assess the accuracy of our SPR results, we measure the absorbance of the inkjet-printed graphene films as a function of the film thickness. The absorbance is measured using a UV−vis spectrometer on the sample shown in Figure 1b. Note that absorbance can also be calculated from the values obtained by SPR and stylus profilometer/AFM measurements. The calculated graphene absorbance, that is, $A = 2 - \log_{10}(T(d)/T_0[\%])$, is obtained from the transmittance using $T(d) = T_0 \exp(-\alpha d)$, where d is the measured film thickness from the stylus profilometer, AFM, or SPR, and α is the absorption coefficient as calculated from the extinction coefficient using the relation $\alpha = 4\pi k/\lambda$. For the stylus profilometer and AFM data, we use the literature value of 1.4 for the extinction coefficient of mechanically exfoliated graphene.[31,35−37] We note that to the best of our knowledge no data on the complex refractive index of inkjet-printed graphene films yet exists.

The comparison between the measured and calculated absorbance is shown in Figure 4. The absorbance increases linearly with increasing number of printing repetitions and is measured as ∼0.18 for the sample with 30 printing repetitions. The absorbance calculated for the same sample according to the SPR results is ∼0.12, slightly smaller than that seen in the absorption measurement. The calculations from the profilometer and AFM data, however, lead to a calculated absorbance of ∼0.45 and ∼0.50 for the same sample, respectively (i.e., >2 times larger than the absorption measurement results). On the other hand, estimation of the thickness of the graphene film deposited with the largest number of printing repetitions from the measured absorbance (by assuming the extinction coefficient of 1.4 for mechanically exfoliated graphene flakes) gives a thickness of ∼10 nm. A layer thickness of ∼10 nm is significantly smaller than that measured by SPR, AFM, and stylus profilometer, strongly suggesting a smaller extinction coefficient for our inkjet-printed graphene layer than that reported in the literature for CVD and micromechanically exfoliated graphene. To estimate this further, we consider the profilometer measured thickness as the correct film thickness and calculate the extinction coefficient value, which gives a similar absorbance to that measured experimentally. This results in an extinction coefficient of ∼0.56 for the sample with 30 printing repetitions. By performing a similar calculation on all the samples, the extinction coefficient of our graphene thin film is estimated to be between 0.5 and 0.6. This is marginally larger but still, notably, in the same range as that obtained from the SPR measurement. Thus, the absorbance values calculated from the SPR results seem to replicate the measured absorbance data better than the stylus profilometer or AFM results combined with the literature values of graphene extinction coefficient. This all provides further evidence for the accuracy of the SPR method for solution deposited material characterization.

We note that the absorbance values reported in this work do not imply that micromechanically exfoliated single layer graphene flakes should absorb less than 2.3% of light or possess a smaller extinction coefficient than the value of 1.4, which is well established.[31,40] The observations of this work only imply that the porous structure of our solution processed graphene film is physically different to that of micromechani-
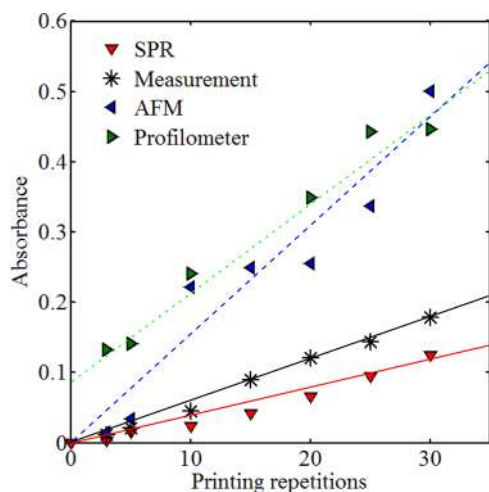
Figure 4. Comparison between the absorbance values measured by UV−vis spectrometer (plotted with black stars) and those calculated from the thickness and the refractive index obtained by SPR and stylus profilometer/AFM measurements. The extinction coefficient used for profilometer and AFM calculations is 1.4[31,35−37] for the data marked with blue and green triangles.

cally exfoliated graphene flakes and CVD graphene films, as was also clearly demonstrated by the optical data gathered by the SPR technique.

CONCLUSIONS

We have shown that SPR can be used to accurately measure the thickness of inkjet-printed graphene thin films. Our results demonstrate that the thickness of graphene thin films has a linear correlation with the number of printing repetitions (∼0.95 nm thickness increase per printing repetition). The thickness obtained by SPR is ∼1.3 and ∼1.5 times smaller than that measured using AFM and the stylus profilometer, respectively. We suggest that the apparent difference is due to the different averaging schemes as the SPR method gives less weight to the surface roughness caused by the isolated and protruding graphene flakes in the porous graphene thin film. In addition to the thickness, the SPR method also reveals the complex refractive index of the thin film, which is significantly lower than that measured from the micromechanically exfoliated or CVD-grown graphene samples. This is due to the high porosity of the thin film resulting from decomposition of the PVP polymer stabilizer in the ink formulation. The extinction coefficient and the thickness values of graphene obtained by SPR measurements match the measured absorbance data better than those obtained using AFM and the stylus profilometer. We therefore strongly believe that SPR could be exploited as a fast, cost-effective, and accurate characterization technique for solution processed graphene thin films.

EXPERIMENTAL METHODS

Information from the SPR Sensors. All samples reported in this work are fabricated on gold coated SPR substrates (or for absorption measurements, directly to microscope slides (Jaytec MBG01012)). First, a chromium adhesion layer (∼2 nm) and a gold layer (∼45 nm) are evaporated on the glass slides using e-beam evaporation at a 0.1−0.2 nm/s rate for both Cr and Au. Information on the two metal layers and the refractive index of each layer (gathered by the quartz crystal

microbalance technique combined with the SPR measurement results) is listed in Table S2. In addition to the printed graphene samples, reference SPR sensors are also needed in the SPR measurements. The used reference sensors are always from the same evaporation batch as the printed graphene samples. Note that we also verified that the SPR spectra of different reference sensors are identical.

Graphene Ink Formulation and Inkjet Printing. Graphene ink is formulated with the UALPE technique. First, 200 mg of graphite crystals (100 mesh flakes; Sigma-Aldrich) and 5 mg of PVP (average molecular weight 10 000 Da; Sigma-Aldrich) are mixed with 20 mL of IPA. The mixture is sonicated in a bath sonicator for 12 h. The bath temperature is kept at ∼15 °C during the exfoliation process. After this, the dispersion is centrifuged for 1 h at 4030 rpm (1540g) to separate the few-layer graphene flakes from the unexfoliated materials. The top 70% of the graphene dispersion is then collected. The graphene ink is stable over several months without the formation of any visible aggregates.

The concentration of dispersed graphene is estimated from the optical absorption of the dispersion via the Beer−Lambert Law. The ink is diluted to 10% v/v to reduce the effects of scattering on the measured absorption.[30] The concentration is estimated (using an absorption coefficient of 2460 L g^{-1} m^{-1} at 660 nm[41,42]) to be 0.59 g L^{-1}.

Sample fabrication by inkjet printing is performed with a DMP-2831 Dimatix Printer. The ink is characterized for its surface tension, density, and viscosity, which can be combined with the nozzle diameter to calculate a figure of merit for jetting stability (Z). The ink surface tension and viscosity are measured using pendant drop measurement and parallel plate rheometer, respectively. The ink density is determined by considering the mass of known volumes of ink. During printing, the substrates are heated to a temperature of 60 °C to promote the evaporation of the ink carrier solvent (IPA). The PVP polymer binder is then decomposed by heating the samples at 400 °C for 30 min. The distribution of flake dimensions (measured via AFM) and the Raman spectra for the ink before and after annealing are presented in Figure S1.

SPR Measurements. SPR measurements are performed in a Kretschmann configuration using a BioNavis MP-SPR Navi 200-L apparatus equipped with 670 and 785 nm light sources. The measurements are performed at 25 °C in ambient air with a ∼0.5 mm diameter measurement beam spot. Therefore, the SPR method gathers information from a large sample area (∼0.2 mm^2), compared to approximately millimeter long tracks for the stylus profilometer, and ∼0.003 mm^2 for AFM. Thus, the information obtained from the spectra represents an average value for the sample.

2 × 2 Transfer Matrix Method (TMM). The 2 × 2 TMM is a simple method to derive the overall reflection and transmission coefficients of a multilayered optical system. In this model, all layers are assumed to be semi-infinite and isotropic, which means the inkjet-printed graphene thin film (as well as the Au and Cr metal layer) is considered to be a homogeneous layer with a specific refractive index and thickness. The relation between the first and the last boundary condition of the N-layered optical system is defined by employing the transfer matrix of the system as follows

$$\begin{bmatrix} \vec{E}_1 \\ \vec{H}_1 \end{bmatrix} = M \begin{bmatrix} \vec{E}_{N-1} \\ \vec{H}_{N-1} \end{bmatrix} \tag{1}$$

where $\vec{E}$ and $\vec{H}$ represent the tangential components of the electric and magnetic fields, respectively, which must be continuous, and M represents the system matrix. By taking the Fresnel equations into account, together with the transfer matrix and the relation of the boundary conditions of the N-layered system, one can derive the overall reflected and transmitted light intensity.[43]

SPR Curve Analysis. The obtained angular spectra are analyzed using a custom software based on *Matlab*, which fits a solution of Maxwell's equation to the measurement results with the help of a *Metropolis* algorithm. During each fitting iteration, the solution to Maxwell's equation is calculated by using a transfer matrix formalism of 2×2 matrices as described above. Thus, the fitting program alters the graphene layer parameters (complex refractive index and the thickness) until a best match between the measurement and the simulation is found. Note that the fitting for the graphene thin film samples is performed with multiple wavelength analysis, assuming the same refractive index of the graphene film for both the measurement wavelengths. This assumption is justified because the complex refractive index of graphene is roughly constant at our measurement range.[20,31,35−37] In addition to this fitting technique, the information from the samples is gathered assuming the same refractive index for all different inkjet-printed graphene layers. This fitting method is referred to as global fitting in the main text. It allows us to estimate the reliability of the values converged by the separate fitting method.

The results obtained by the custom software are compared to those from commercial *BioNavis LayerSolver* software and *Winspall* freeware; and the results are observed to match well. Our software is based on the *Metropolis* algorithm which, whilst converging toward a best fit solution, changes the complex refractive index and the thickness of inkjet-printed graphene layers. The advantage gained by using the *Metropolis* algorithm in the fitting is that it prevents the fitting software from converging to a local minimum, which can happen because during iteration occasionally a bad solution will be accepted. By doing so, the algorithm is capable of pushing itself outside of the local minima and continues the iteration until a global solution to the fitting problem is determined. We note that the optical information of the SPR measurement substrate also strongly influences the calculated SPR curve (i.e., the thickness and refractive index of all the other layers in the sensor structure). Therefore, to ensure maximum accuracy, background scans and fits for the uncoated SPR substrates are performed prior to the graphene deposition. The optical information obtained from these fits is provided in the Table S2.

AFM and Stylus Profilometer. AFM and stylus profilometer measurements are performed to estimate the thickness of the printed graphene thin films. AFM imaging is performed using a Bruker Dimension Icon setup operated in PeakForce mode. The maximum scan area measured using the AFM is 50 μm $\times$ 50 μm. Profilometry measurements are performed with a Bruker DektakXT stylus profilometer using line scans of distances between 1.0 and 2.0 mm. By way of post-measurement processing, the AFM images are corrected with a flattening algorithm, fitting each individual line data to a first-order curve and then a second-order curve to subtract the sample tilt and surface bowing, respectively. Stylus profilometer line scans are leveled with respect to the quasi-linear, horizontal profile of the glass substrate.

Optical Absorbance. Optical absorbance of the fabricated graphene samples is measured with a standard UV−vis spectrometer as a function of inkjet-printed film thickness. For the measurement, 1−30 printing repetitions of graphene are printed on the microscope slide and the absorbance recorded. The microscope slide absorbance is subtracted from the measured values.

Raman Spectroscopy. Raman measurements are performed using a Renishaw InVia microspectrometer at an excitation wavelength of 514 nm, to demonstrate that inkjet-printed graphene film is composed of graphene flakes. Spectra are acquired at room temperature in a backscattering geometry using a 100$\times$ microscope objective lens with a spot size of $\sim$1 μm^2. The power on the sample is $\sim$0.01 mW.

ASSOCIATED CONTENT

⑤ Supporting Information

The Supporting Information is available free of charge on the ACS Publications website at DOI: 10.1021/acsomega.7b00336.

> Extra information from graphene ink used in the fabrication of the graphene films; fitting analysis using the global fitting technique; comparison between the AFM, SPR, and stylus profilometer measurement areas (PDF)

AUTHOR INFORMATION

Corresponding Authors
*E-mail: henri.jussila@aalto.fi (H.J.).
*E-mail: th270@cam.ac.uk (T.H.).

Notes

The authors declare no competing financial interest.

ACKNOWLEDGMENTS

REFERENCES

(1) Ferrari, A. C.; et al. Science and Technology Roadmap for Graphene, Related Two-Dimensional Crystals and Hybrid Systems. *Nanoscale* **2015**, 7, 4598−4810.

(2) Novoselov, K. S.; Geim, A. K.; Morozov, S. V.; Jiang, D.; Zhang, Y.; Dubonos, S. V.; Grigorieva, I. V.; Firsov, A. A. Electric Field Effect in Atomically Thin Carbon Crystals. *Science* **2004**, 306, 666−669.

(3) Bolotin, K. I.; Sikes, K. J.; Jiang, Z.; Klima, M.; Fudenberg, G.; Hone, J.; Kim, P.; Stormer, H. L. Ultrahigh Electron Mobility in Suspended Graphene. *Solid State Commun.* **2008**, 146, 351−355.

(4) Sun, Z.; Hasan, T.; Torrisi, F.; Popa, D.; Privitera, G.; Wang, F.; Bonaccorso, F.; Basko, D. M.; Ferrari, A. C. Graphene Mode-Locked Ultrafast Lasers. *ACS Nano* **2010**, *4*, 803–810.

(5) Bonaccorso, F.; Sun, Z.; Hasan, T.; Ferrari, A. C. Graphene Photonics and Optoelectronics. *Nat. Photonics* **2010**, *4*, 611–622.

(6) Balandin, A. A.; Ghosh, S.; Bao, W.; Calizo, I.; Teweldebrhan, D.; Miao, F.; Lau, C. N. Superior Thermal Conductivity of Single-Layer Graphene. *Nano Lett.* **2008**, *8*, 902–907.

(7) Wang, Q. H.; Kalantar-Zadeh, K.; Kis, A.; Coleman, J. N.; Strano, M. S. Electronics and Optoelectronics of Two-Dimensional Transition Metal Dichalcogenides. *Nat. Nanotechnol.* **2012**, *7*, 699–712.

(8) Xia, F.; Wang, H.; Jia, Y. Rediscovering Black Phosphorus as an Anisotropic Layered Material for Optoelectronics and Electronics. *Nat. Commun.* **2014**, *5*, No. 4458.

(9) Li, L.; Yu, Y.; Ye, G. J.; Ge, Q.; Ou, X.; Wu, H.; Feng, D.; Chen, X. H.; Zhang, Y. Black phosphorus Field Effect Transistors. *Nat. Nanotechnol.* **2014**, *9*, 372.

(10) Nicolosi, V.; Chhowalla, M.; Kanatzidis, M. G.; Strano, M. S.; Coleman, J. N. Liquid Exfoliation of Layered Materials. *Science* **2013**, *340*, 1420.

(11) Torrisi, F.; Hasan, T.; Wu, W.; Sun, Z.; Lombardo, A.; Kulmala, T. S.; Hsieh, G-W; Jung, S.; Bonaccorso, F.; Paul, P. J.; Chu, D.; Ferrari, A. C. Inkjet-Printed Graphene Electronics. *ACS Nano* **2012**, *6*, 2992–3006.

(12) Li, J.; Ye, F.; Vaziri, S.; Muhammed, M.; Lemme, M. C.; Östling, M. Efficient Inkjet Printing of Graphene. *Adv. Mater.* **2013**, *25*, 3985.

(13) Löfås, S.; Malmqvist, M.; Rönnberg, I.; Stenberg, E.; Liedberg, B.; Lundström, I. Bioanalysis with Surface Plasmon Resonance. *Sens. Actuators, B* **1991**, *5*, 79.

(14) Granqvist, N.; Liang, H.; Laurila, T.; Sadowski, J.; Yliperttula, M.; Viitala, T. Characterizing Ultrathin and Thick Organic Layers by Surface Plasmon Resonance Three Wavelength and Waveguide Mode Analysis. *Langmuir* **2013**, *29*, 8561–8571.

(15) Vikholm-Lundin, I.; Albers, W. M. Surface Plasmon Resonance on Nano-scale Organic Films. In *Nano-Bio-Sensing*; Carrara, S., Ed.; Springer, 2010; pp 83–125.

(16) Sadowski, J. W.; Korhonen, I. K.; Peltonen, J. P. Characterization of Thin Films and Their Structures in Surface Plasmon Resonance Measurements. *Opt. Eng.* **1995**, *34*, 2581–2586.

(17) Wu, L.; Chu, H. S.; Koh, W. S.; Li, E. P. Highly Sensitive Graphene Biosensors Based on Surface Plasmon Resonance. *Opt. Express* **2010**, *18*, 14395.

(18) Szunerits, S.; Maalouli, N.; Wijaya, E.; Vilcot, J. P.; Boukherroub, R. Recent Advances in the Development of Graphene Based Surface Plasmon Resonance Interfaces. *Anal. Bioanal. Chem.* **2013**, *405*, 1435–1443.

(19) Salihoglu, O.; Balci, S.; Kocabas, C. Plasmon-Polaritons on Graphene-Metal Surface and Their Use in Biosensors. *Appl. Phys. Lett.* **2012**, *100*, No. 213110.

(20) Jussila, H.; Yang, H.; Granqvist, N.; Sun, Z. Surface Plasmon Resonance for Characterization of Large-Area Atomic-Layer Graphene Film. *Optica* **2016**, *3*, 151.

(21) He, X.; Zhao, Z.-Y.; Shi, W. Graphene Supported Tunable Near-IR Metamaterials. *Opt. Lett.* **2015**, *40*, 178–181.

(22) He, X.; Kim, S. Tunable Terahertz Graphene Metamaterials. *Carbon* **2015**, *82*, 229.

(23) He, X.; Gao, P.; Shi, W. A Further Comparison of Graphene and Thin Metal Layers for Plasmonics. *Nanoscale* **2016**, *8*, 10388–10397.

(24) Mertens, J.; Eiden, A. L.; Sigle, D. O.; Huang, F.; Lombardo, A.; Sun, Z.; Sundaram, R. S.; Colli, A.; Tserkezis, C.; Aizpurua, J.; Milana, S.; Ferrari, A. C.; Baumberg, J. J. Controlling Subnanometer Gaps in Plasmonic Dimers Using Graphene. *Nano Lett.* **2013**, *13*, 5033–5038.

(25) Grigorenko, A. N.; Polini, M.; Novoselov, K. S. Graphene Plasmonics. *Nat. Photonics* **2012**, *6*, 749–758.

(26) Santra, S.; Hu, G.; Howe, R. C. T.; De Luca, A.; Ali, S. Z.; Udrea, F.; Gardner, J. W.; Ray, S. K.; Guha, P. K.; Hasan, T. CMOS Integration of Inkjet Printed Graphene for Humidity Sensing. *Sci. Rep.* **2015**, *5*, No. 17374.

(27) Hansen, C. M. *Hansen Solubility Parameters: A User's Handbook*, 2nd ed.; CRC Press, Inc.: Boca Raton, FL, 2007; pp 4–6.

(28) Hernandez, Y.; Lotya, M.; Rickard, D.; Bergin, S. D.; Coleman, J. N. Measurement of Multicomponent Solubility Parameters for Graphene Facilitates Solvent Discovery. *Langmuir* **2010**, *26*, 3208.

(29) Howe, R. C. T.; Hu, G.; Yang, Z.; Hasan, T. Functional Inks of Graphene, Transition Metal Dichalcogenides and Black Phorsphorus for Photonics and (Opto)Electronics. *Proc. SPIE* **2015**, *9553*, No. 95530R.

(30) Bohren, C. F.; Huffman, D. F. *Absorption and Scattering of Light by Small Particles*; Wiley, 1998.

(31) Kravets, V. G.; Grigorenko, A. N.; Nair, R. R.; Blake, P.; Anissimova, S.; Novoselov, K. S.; Geim, A. K. Spectroscopic Ellipsometry of Graphene and Exciton-Shifted van Hove Peak in Absorption. *Phys. Rev. B: Condens. Matter Mater. Phys.* **2010**, *81*, No. 155413.

(32) Gupta, A.; Chen, G.; Joshi, P.; Tadigadapa, S.; Eklund, P. C. Raman Scattering from High-Frequency Photons in Supported n-Graphene Layer Films. *Nano Lett.* **2006**, *6*, 2667–73.

(33) Hutchings, M.; Martin, G. D. *Inkjet Technology for Digital Fabrication*; John Wiley Sons, 2012; pp 21–26.

(34) Dodoo-Arhin, D.; Howe, R. C. T.; Hu, G.; Zhang, Y.; Hiralal, P.; Bello, A.; Amaratunga, G.; Hasan, T. Inkjet Printed Graphene Electrodes for Dye-Sensitized Solar Cells. *Carbon* **2016**, *105*, 33.

(35) Bruna, M.; Borini, S. Optical Constants of Graphene Layers in the Visible Range. *Appl. Phys. Lett.* **2009**, *94*, No. 031901.

(36) Nelson, F. J.; Kamineni, V. K.; Zhang, T.; Comfort, E. S.; Lee, J. U.; Diebold, A. C. Optical Properties of Large Area Polycrystalline Chemical Vapor Deposited Graphene by Spectroscopic Ellipsometry. *Appl. Phys. Lett.* **2010**, *97*, No. 253110.

(37) Weber, J. W.; Calado, V. E.; van de Sanden, M. C. M. Optical Constants of Graphene Measured by Spectroscopic Ellipsometry. *Appl. Phys. Lett.* **2010**, *97*, No. 091904.

(38) Pap, A. E.; Kordas, K.; Vähäkangas, J.; Uusimäki, A.; Leppävuori, S.; Pilon, L.; Szatmari, S. Optical Properties of Porous Silicon. Part III: Comparison of Experimental and Theoretical Results. *Opt. Mater.* **2006**, *28*, 506.

(39) Yamaguchi, M.; Nakayama, H.; Yamada, K.; Imai, H. Ultralow Refractive Index Coatings Consisting of Mesoporous Silica Nanoparticles. *Opt. Lett.* **2009**, *34*, 2060–2062.

(40) Nair, R. R.; Blake, P.; Grigorenko, A. N.; Novoselov, K. S.; Booth, T. J.; Stauber, T.; Perez, N. M. R.; Geim, A. K. Fine Structure Constant Defines Visual Transparency of Graphene. *Science* **2008**, *320*, 1308.

(41) Hasan, T.; Torrisi, F.; Sun, Z.; Popa, D.; Nicolosi, V.; Privitera, G.; Bonaccorso, F.; Ferrari, A. C. Solution Phase Exfoliation of Graphite for Ultrafast Photonics. *Phys. Status Solidi B* **2010**, *247*, 2953–2957.

(42) Hernandez, Y.; Nicolosi, V.; Lotya, M.; Blighe, F. M.; Sun, Z.; De, S.; McGovern, I. T.; Holland, B.; Byrne, M.; Gun'Ko, Y. K.; Boland, J. J.; Niraj, P.; Duesberg, G.; Krishnamurthy, S.; Goodhue, R.; Hutchison, J.; Scardaci, V.; Ferrari, A. C.; Coleman, J. N. High Yield Production of Graphene by Liquid Phase Exfoliation of Graphite. *Nat. Nanotechnol.* **2008**, *3*, 563–568.

(43) Hansen, W. M. Electric Fields Produced by the Propagation of Plane Coherent Electromagnetic Radiation in a Stratified Medium. *J. Opt. Soc. Am.* **1968**, *58*, 380.